J. Fluid Mech. (2009), *vol.* 628, *pp.* 43–55.
doi:10.1017/S0022112009006156 Printed in the United Kingdom

Experimental and numerical study of miscible Faraday instability

F. ZOUESHTIAGH[1]†, S. AMIROUDINE[2] AND R. NARAYANAN[3]

[1]Institut d'Electronique, de Microélectronique et de Nanotechnologie UMR CNRS 8520, Avenue Poincaré, 59652 Villeneuve d'Ascq, France

[2]LPMI-Arts et Métiers ParisTech., 2 Bd du Ronceray, BP 93525, 49035 Angers, France

[3]University of Florida, Department of Chemical Engineering, Gainesville, FL 32611-6005, USA

(Received 3 September 2008 and in revised form 15 January 2009)

A study of the Faraday instability of diffuse interfaces between pairs of miscible liquids of different densities, by means of experiments and by a nonlinear numerical model, is presented. The experimental set-up consisted of a rectangular cell in which the lighter liquid was placed above the denser one. The cell in this initially stable configuration was then subjected to vertical vibrations. The subsequent behaviour of the 'interface' between the two liquids was observed with a high-speed camera. This study shows that above a certain acceleration threshold an instability developed at the interface. The amplitude of the instability grew during the experiments which then led to the mixing of the liquids. The instability finally disappeared once the two liquids were fully mixed over a volume, considerably larger than the initial diffuse region. The results of a companion two-dimensional nonlinear numerical model that employs a finite volume method show very good agreement with the experiments. A physical explanation of the instability and the observations are advanced.

1. Introduction

The instability of a vibrating liquid layer with a free surface leads to Faraday waves. The waves between phases of different densities are excited by inertial forces (see Faraday 1831; Benjamin & Ursell 1954). Short wavelength disturbances are stabilized by surface tension and by the dissipation of momentum via viscous relaxation while they are destabilized by transverse variations in surface elevation which, in turn, lead to transverse variation in inertial forces. These forces are excited by the external vibrations. It is this competition between the stabilizing and destabilizing effects that leads to the selection of patterns with finite wavelengths when a liquid with a free surface is subject to vibrations. Since Faraday's work, numerous studies have been done on various aspects of vertical vibrations on liquid layers, films or drops. These studies have led to a better understanding of fluid behaviour and consequently have paved the way for new industrial processes. For instance, James *et al.* (2003) and Zoueshtiagh *et al.* (2006) have shown novel methods for atomizing liquid drops or air bubbles by bursting them using vibrations. By this means, the bubble or drop generation and sizes can be better controlled. This in turn has potential application to pharmaceutical production. Other work related to the current study is the parametric

† Email address for correspondence: Farzam.Zoueshtiagh@univ-lille1.fr

instability of a liquid–vapour interface close to the critical point where the surface tension approaches zero (Fauve *et al.* 1992). In addition to this work are the studies of instability due to mechanical vibrations in systems where low surface tension arises from the addition of surfactants (Kumar & Matar 2004; Ubal, Giavedoni & Saita 2005*a*, *b*; Ballesta & Manneville 2006).

Experiments on the Faraday instability in immiscible fluid layers have been performed (Tipton & Mullin 2004) with a view of understanding interfacial modulation on an acceleration-driven instability while offering confirmation of established theories (Kumar & Tuckerman 1994). Now much of the earlier work has centred on immiscible fluid layers and it is somewhat surprising that the analogous problem for miscible layers has been less studied. The miscible fluid problem is different from the usual Faraday instability described earlier as here we do not have a clearly demarked interface with a companion interfacial tension. In the miscible case there is the diffusion of momentum and species to stabilize the diffuse region while in the immiscible system diffusion of momentum via the kinematic viscosity and interfacial tension are the agents of stabilization. In the miscible fluid case there are no distinct surface elevations or depressions that can cause inertial forcing from external acceleration unlike the immiscible case. Instead the destabilization effect of short wavelengths is thought to occur from the transverse variation of density. In other words the destabilization of a diffuse interface in the presence of vibration is akin to the Bénard instability where even an erstwhile quiescent layer that is stably stratified can experience sustained flow when subjected to inertial vibrations (Shukla & Narayanan 2002). In such a problem the larger the external acceleration the smaller the wavelength at the onset of the instability.

The differences between Faraday instability in immiscible and miscible systems are not restricted only to the nature of the interface, being singular in one case and diffuse in the other, but also to the nature of the potential that drives the instability in the first place. In an immiscible system it is enough to have a jump discontinuity in density at the surface. In a miscible system one needs a gradient of density to drive the instability. These density gradients can be caused by temperature or concentration fields. Once the instability sets in, the gradients begin to weaken as a result of convective mixing. This in turn causes the waves that characterize the secondary motion, to disappear. In other words the miscible layer Faraday problem is necessarily transient and can never attain a periodic steady state unlike its immiscible counterpart.

The current study is an attempt to provide experimental evidence for the Faraday instability in miscible fluids. Experiments on several systems of miscible fluids will be discussed and for each the principal input variables are the amplitude and frequency of the imposed oscillation, while the output is the wavelength of the diffuse interface. The variation of the wavelength with the time, after the miscible fluids first make contact, as well as the mean viscosity of the fluids are discussed in addition to the frequency of the response. Our observations are qualitatively compared with a two-dimensional nonlinear model that is solved numerically. The transient nature of the instability will be seen in the experiments and in the computations. We will also see that the frequency of the response is half of the imposed frequency. For all of these observations physical explanations are advanced. We now turn to the discussion of the experiments and to the model.

2. The experimental set-up

The main idea behind the experiments is to determine the regimes for which a pair of stably stratified miscible fluid layers subjected to vertical vibrations becomes

Fluid	Kinematic viscosity ($m^2\,s^{-1}$)	Specific gravity
Pure water	0.9×10^{-6}	1.0
Salt saturated water	1.7×10^{-6}	1.2 (Lide 2004)
1 cSt Silicone oil	1×10^{-6}	0.826
2 cSt Silicone oil	2×10^{-6}	0.87
5 cSt Silicone oil	5×10^{-6}	0.92
10 cSt Silicone oil	10×10^{-6}	0.93
50 cSt Silicone oil	50×10^{-6}	0.96

TABLE 1. Physical properties of different fluids used in the experiments. The silicone oils are completely miscible in one another. The same is true of brine and fresh water.

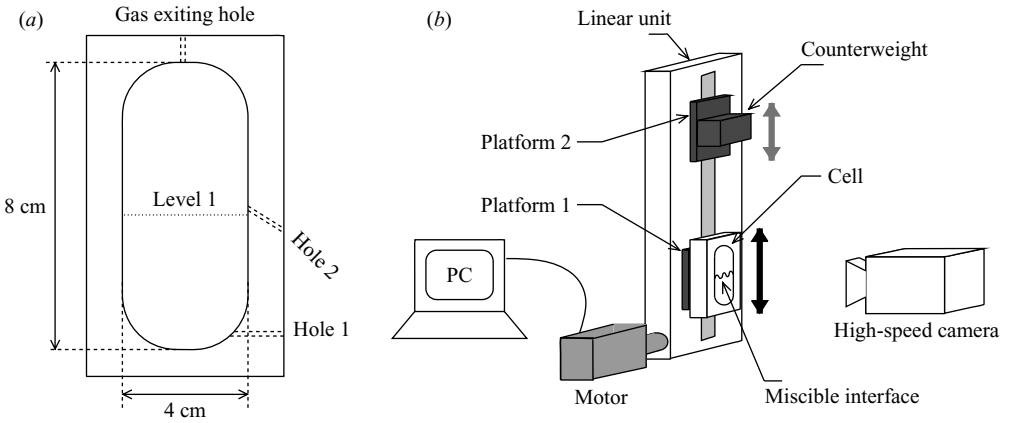

FIGURE 1. Sketch of (*a*) the test cell and (*b*) the experimental set-up.

unstable. The instability is manifested by the onset of wavy motion with a definite wavelength λ in the region of the diffuse interface. To this end an apparatus was constructed wherein the heavier fluid was inserted first and the lighter fluid was placed very gently above it. Two different systems of fluids were chosen, the first being de-ionized water and salt-saturated water; the second, sets of two different silicone oils of disparate densities. Their relevant properties are given in table 1.

The test cell depicted in figure 1(*a*) consisted of a Plexiglas cell of $8 \times 4 \times 2$ cm^3 which was filled until level 1 with the heavier of the two fluids. From level 1 to the top, the cell was filled through the side hole 2 with the lighter of the two fluids. Because of the density gradient between the two liquids at their interface, the latter was easily observable with ordinary lighting. The cell was usually shaken 5 min after the start of injection of the lighter fluid into the cell. This time corresponded to the time necessary to slowly fill the cell without drastically perturbing the interface. Air bubbles inside the cell were evacuated via the vent or 'gas exiting hole' at the top of the cell (see figure 1*a*). This vent was blocked with a screw once the cell was completely filled. The thickness of the diffuse interface region prior to shaking was estimated to be of the order of millimetres. The motion of the interface was observed by a high-speed camera at either 150, 200 or 250 images per second with an exposure time of 250 μs. The recorded images were digitized and calibrated into length scales from which the size of the instability (wavelengths) was measured. The error in wavelength measurements was estimated to be about $\pm 5\,\%$.

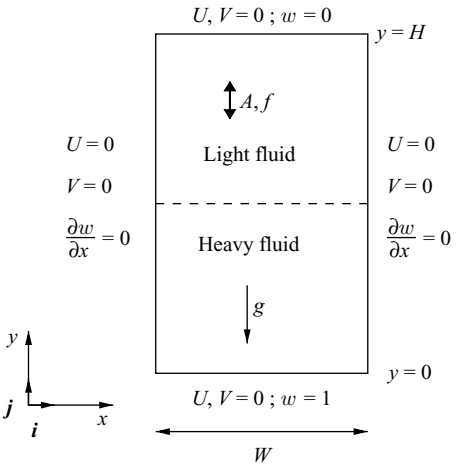

FIGURE 2. The geometry and the boundary conditions of the numerical problem.

The set-up providing the oscillations to the cell is shown in figure 1(*b*). It consisted of a linear unit system connected to a SGMPH-04AA Fenwick servomotor. The system converted the rotating motion of the drive pin into a linear movement of the guide platforms 1 and 2. The test cell was attached to the lower sliding plate, i.e. platform 1 while on platform 2 a counterweight of the cell was mounted. The platforms were moved to the middle or apart simultaneously. This anti-phase movement combined with the presence of the counterweight was aimed at reducing the vibrations transmitted to the frame structure. The motion of the drive was computer controlled and allowed oscillation amplitudes A in the range $0.75 \leqslant A \leqslant 10$ cm, and frequencies f, $f \leqslant 10$ Hz. The accuracy of the amplitudes and frequencies were held to within ± 1 mm and $\pm 1/60$ Hz, respectively. The drive motion, hence the movement of the unit, could provide sinusoidal motions at speeds of up to 5 m s^{-1} and accelerations typically up to ≈ 35 m s^{-2}.

To help understand the experimental results we now advance a simplified numerical model with all of the essential physics. The aim of the calculations is to explain the onset of the instability, the prediction of the wavelength evolution in time and the occurrence of an observed period doubling behaviour in the ensuing motion.

3. The mathematical model

The experiment is modelled mathematically as a two-dimensional rectangular cavity enclosing two fluids. It is depicted in figure 2. The height of the cavity is H, its width is W and the entire container is subjected to vertical vibration with amplitude A and frequency f. The lower fluid is the heavier one with the heavy species denoted by the subscript 'I'. The fluid is assumed to be Newtonian and the density is taken to be a function of the mass fraction of the species. Denoting 'L' as a length scale, to be defined momentarily, the scaled equations are written as

$$\left.\begin{aligned} \frac{\partial \rho}{\partial t} + \nabla \cdot (\rho \boldsymbol{V}) &= 0 \\ \rho \left[\frac{\partial \boldsymbol{V}}{\partial t} + (\boldsymbol{V} \cdot \nabla)\boldsymbol{V} \right] &= -\nabla P + \frac{1}{Re}[\Delta \boldsymbol{V}] - \rho \left(\frac{1}{Fr^2} - \frac{1}{Fr_v^2} \sin(W_0 t) \right) \boldsymbol{j} \\ \rho \left(\frac{\partial w}{\partial t} + \boldsymbol{V} \cdot \nabla w \right) &= \frac{1}{Re\, Sc} \nabla \cdot \rho [\nabla w] \end{aligned}\right\} \quad (3.1)$$

These equations are subject to the scaled boundary conditions given by

$$\left.\begin{array}{llll} y = 0, & U = 0, & V = 0, & w = 1, \\ y = H/L, & U = 0, & V = 0, & w = 0, \\ x = 0, W/L, & U = 0, & V = 0, & \dfrac{\partial w}{\partial x} = 0. \end{array}\right\} \tag{3.2}$$

In the above equations, $\boldsymbol{V}$ is the scaled velocity vector whose horizontal and vertical components are denoted by U and V, respectively. Also in the above equations, the scaled mixture density and mass fraction of the heavier species are correspondingly denoted by ρ and w. The scale factor for the mixture density is the density of the heavy species (brine say), denoted by ρ_I. The scaled mixture density ρ is then determined by $\rho = 1 + \gamma(w - 1)$ where $\gamma = (\rho_I - \rho_{II})/\rho_I$ with the density of the light species (pure water say) being denoted by ρ_{II} .

To render the modelling equations in scaled form, requires us to define length, time and velocity scales. The length scale 'L', left unspecified until now, is hereafter given by $\sqrt{Dt_0}$. The time scale is given by $t_{ref} = L^2/\nu$ and the velocity scale by $U_{ref} = \nu/L$ where D and ν are the mass or solutal diffusivity and kinematic viscosity, respectively.

Observe that $\sqrt{Dt_0}$ is a solutal diffusion length, where t_0 is the initial experimental wait time before the oscillations are imposed. In the experiments, t_0 was typically 300 s and it is this value that is assumed in all of the computations in order to make qualitative comparisons with the observations. This value of t_0 yields a solutal diffusive length of the order of about 1/2 mm, a small number in comparison with the cell dimensions. Also observe that the characteristic time scale is essentially a viscous scale even though the characteristic length scale is related to solutal diffusion. The reason for this choice emanates from our view of the problem. The imposed oscillations are time periodic mechanical inputs that can be dissipated by viscosity whereas the instability finds its roots in transverse variations of concentration or density so that all lengths including wavelengths seen at instability ought to reasonably scale with the solutal diffusive distance.

The different dimensionless coefficients appearing in the above equations are the following: $Fr = U_{ref}/\sqrt{Lg}$ (Froude number), $Sc = \nu/D$ (Schmidt number), $W_0 = 2\pi f t_{ref}$ (Womersley number), $Re = LU_{ref}/\nu$ (Reynolds number) and $Fr_v = U_{ref}/\sqrt{LA(2\pi f)^2}$ (vibration Froude number). We see that the scale factors make the Reynolds number Re equal to unity. In other words viscous damping of disturbances is never ignored in this model. Other dimensionless groups occurring in the study are the Womersley number, which is a scaled frequency, and the ratio of the two Froude numbers. The Womersley number provides a guide to the frequency at which instability can be expected if the viscosity were increased. It provides the penetration depth of the momentum boundary layer. The ratio of the Froude numbers provides a guide to the amplitude that is needed in order to keep the externally imposed acceleration invariant when the frequency is changed. An increase in the vibrational Froude number is the principal reason for the instability; as such an increase acts to enhance the inertial instability of a wave at the diffuse interface in the face of a perturbation. The scaled equations will also give rise to a Schmidt number. Its role is dual. Holding all other groups fixed, a small Schmidt number indicates a large diffusion coefficient compared to the kinematic viscosity. This will lead to the appearance of an instability early in time as a concentration gradient is initially established, while a homogeneous concentration field will develop at longer times. A large Schmidt number has the opposite effect.

The domain equations are solved under the conditions that the top and bottom walls are rigid, horizontal and maintained at constant concentration. While the last two restrictions are not quite satisfied experimentally they are nonetheless approximately true, as the characteristic diffusional lengths were much smaller than the vertical dimension of the cell in our experiments.

Equations (3.1) and (3.2) are solved with a finite volume method using the SIMPLER algorithm (Patankar 1980; Amiroudine *et al.* 1997) in a staggered mesh. The space discretization uses the power-law scheme (Patankar 1980) and time discretization is of the first-order Euler type. As the characteristic time t_0 and consequently the characteristic length, which is the diffusive length, are assumed to be small the numerical calculations assume that the oscillations commence immediately after the fluids make contact. The numerical code used here was bench marked and tested against several problems such as the Bénard problem and problems with compressible (perfect gases) or highly compressible (supercritical) fluids (Amiroudine *et al.* 1997, 2001; Amiroudine & Zappoli 2003). The effect of the grid size was also carefully tested for convergence. A non-uniform mesh is used in order to capture the phenomena at the interface and near the walls. Observe that the vibrational boundary layer thickness is of the order of $\delta_{vib} \approx \sqrt{\nu/\pi f} \approx 200$ μm for a maximum frequency of $f = 8$ Hz and kinematic viscosity of 1 cSt. Therefore, for all cases the non-uniform mesh has 80×80 points and the first point of the mesh is at around 150 μm. An increase in mesh points did not change the results of the calculation indicating that the vibrational boundary layer was well resolved by the numerical scheme. The time step chosen is equal to 10^{-3} s, which is very small with respect to all of the characteristic time scales.

4. A discussion of the numerical calculations and experimental observations

The calculations were done for two sets of fluids viz. (i) brine and pure water with kinematic viscosity of $\nu \approx 10^{-6}$ m^2 s^{-1}, solute diffusivity of $D \approx 10^{-9}$ m^2 s^{-1} and $(\rho_I - \rho_{II})/\rho_I = 0.16$, (ii) silicone oils with $\nu \approx 6.7 \times 10^{-6}$ m^2 s^{-1}, $D \approx 10^{-9}$ m^2 s^{-1} and $(\rho_I - \rho_{II})/\rho_I = 6.2 \times 10^{-2}$. In the second case, we assumed the viscosities to be of the same order for the two fluids even though they were quite different in the experiment. This is permissible because the real cause of the instability is the difference in densities as noted in § 1. The effect of mean viscosity on the wavelength of the instability will be discussed later in the paper.

Figure 3 shows the time evolution of the density field for the water/brine case using a vibration amplitude of 1 cm and a frequency of 8 Hz. At early times ($t = 0.65$ s), the profile is purely diffusive which means that at very short times the instability cannot establish itself since the dimension of the diffuse interface is extremely small. Since the instability is, in principle, similar to the Bénard instability a short diffusion length can only offer stabilization. As the oscillations continue in time, a wavy instability appears at $t = 0.82$ s starting from the boundaries. Then at $t = 1.35$ s, the whole interface is unstable with a clear wavelength. But if the oscillations continue for a long time, the density gradients become smeared on account of mixing; consequently the instability disappears. Therefore, the instability is really one which appears over a transient period.

To see whether the numerical observations are qualitatively similar to those made in the experiments we consider several photographs of experimental runs (see also attached movies 1 and 2 [available with the online version of this paper]). The pictures depict results from the brine/water case. The oil/oil case was qualitatively

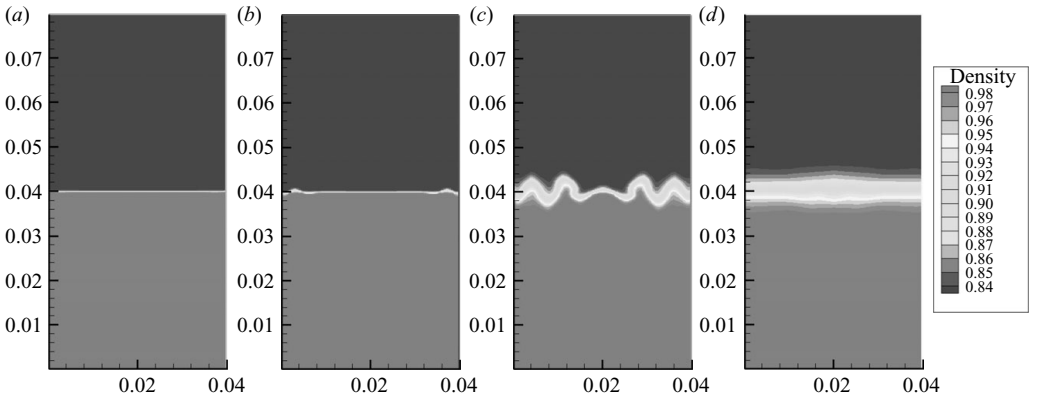

FIGURE 3. Time evolution of the density field for the case of water–brine with a vibration of an amplitude of 1 cm and a frequency of 8 Hz; (*a*) $t = 0.65$ s, (*b*) $t = 0.82$ s, (*c*) $t = 1.35$ s and (*d*) $t = 3.42$ s. The wavelength deduced from (*c*) is about 0.7 cm.

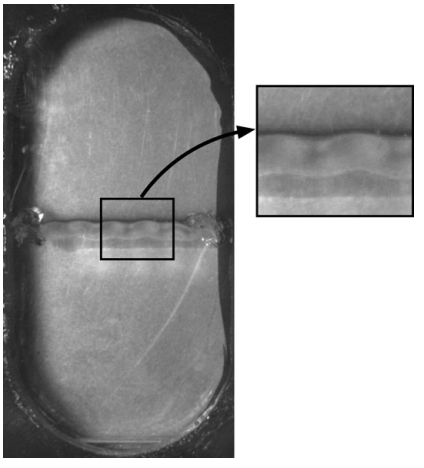

FIGURE 4. Photograph of the instability observed at the interface. Experimental parameters: $A = 1$ cm, $f = 8$ Hz and waiting time $t_0 = 5$ min. The measured wavelength in the picture is about 0.6 cm.

very similar. Figure 4 shows a photograph of the instability developing with small wavelengths. The experimental wavelengths in this figure are of comparable value to those from the numerical calculations shown in figure 3. The amplitude and the frequency of the imposed oscillations in this comparison are the same.

The set of photographs in figure 5, obtained here for $A = 10$ cm and $f = 1.5$ Hz, shows the behaviour of the interface at different times ($t = 0$ refers to the beginning of the shaking) during the experiment. In this figure one can see that the interface between the two liquids was smooth and clear at the beginning of the shaking and as time increased the instability developed and the interface became thicker because of the mixing. At the end of the experiment the two liquids spread into each other over the entire cell. Such large spreading was not always the case. For instance, at small amplitudes the spreading was usually confined to near the centre of the cell. This situation, which is comparable to a diffusion-thickened interface for large initial waiting periods, could sometimes lead to the formation of another wavelength during

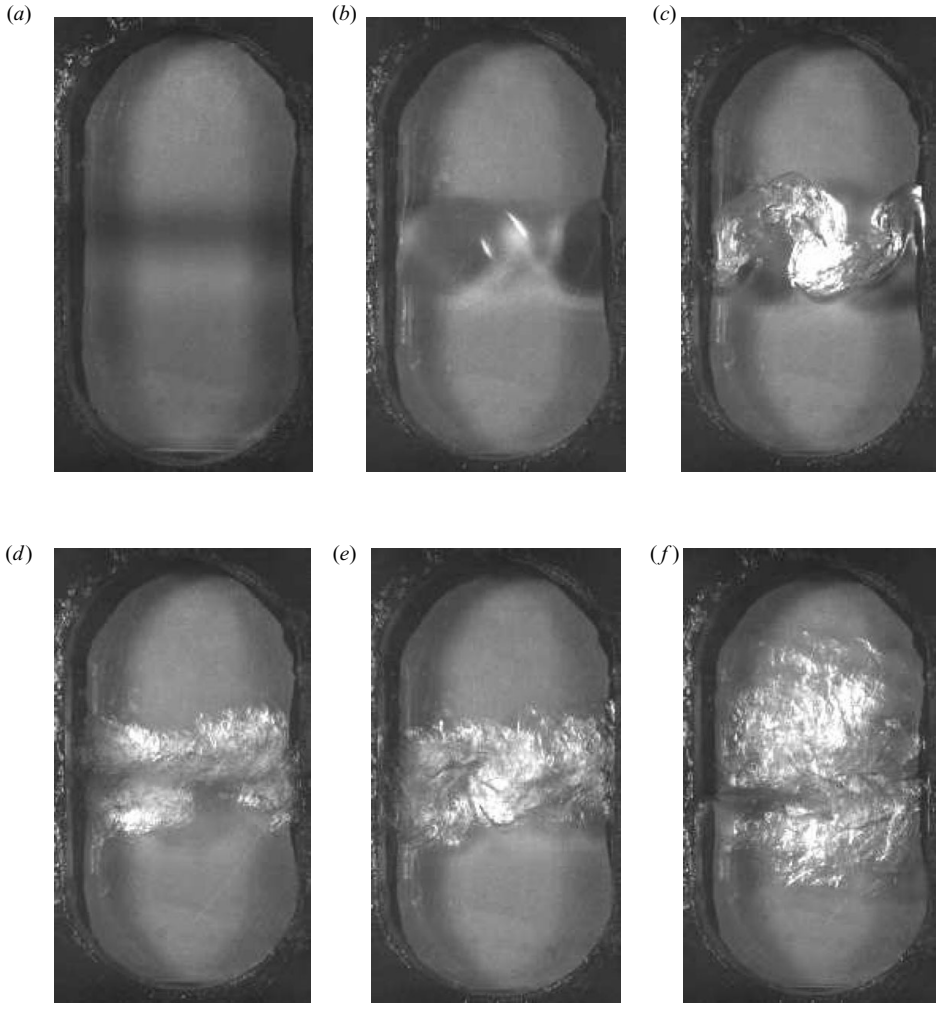

FIGURE 5. Image sequence of interface evolution during an experiment; (*a*) $t = 0$ s, (*b*) $t = 4.98$ s, (*c*) $t = 6.32$ s, (*d*) $t = 6.74$ s, (*e*) $t = 6.98$ s and (*f*) $t = 11.68$ s. Experimental parameters: $A = 10$ cm, $f = 1.5$ Hz and $t_0 = 75$ min.

the same experiment but only at large t (see movie 2). Unfortunately, the memory limitations of the camera did not allow further exploration of this phenomena.

Now each experiment was begun after a definite waiting period. This waiting period was the time needed to fill the cell with the upper fluid after it first made contact with the heavy fluid below it. The effect of this waiting period, called t_0, on the wavelength of the instability is of interest. Figure 6 shows a sequence of images with a vibration of amplitude 10 cm and frequency of 1.5 Hz for different waiting periods. A plot of the wavelength change with wait time for a few values of acceleration is depicted in figure 7. As t_0 is the characteristic time this plot is shown unscaled. This figure should be viewed with some caution since long wait times, greater than 75 min, would encourage the influence of the horizontal dimensions on the wavelength due to the large diffusion lengths. The message of this plot is that the wavelength decreased with increasing t_0. This observation is reasonable as large

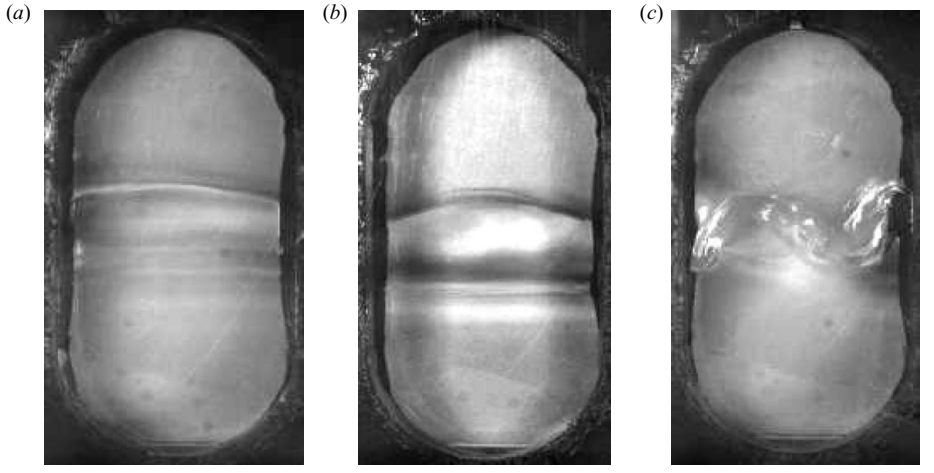

FIGURE 6. Influence of the wait time t_0 before the start of experiment on the developing wavelength. Experimental parameters: $A = 10$ cm, $f = 1.5$ Hz (*a*) $t_0 = 5$ min, (*b*) $t_0 = 20$ min and (*c*) $t_0 = 45$ min.

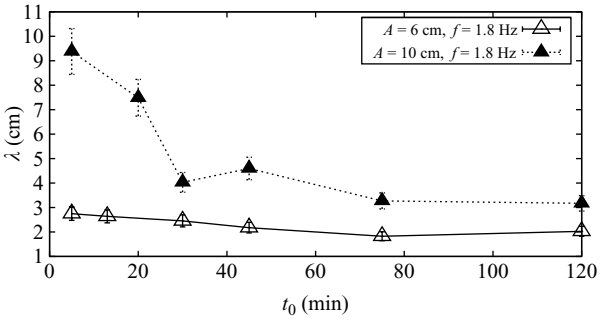

FIGURE 7. Wavelength as a function of wait time t_0 before the start of the experiment.

waiting periods would lead to weaker initial concentration gradients and this in turn would require sharper transverse density gradients to get the instability going. In other words short wavelengths must come attendant with large wait times due to weak driving potentials.

A curious observation that was made during the experiment was the appearance of 'secondary waves'. These waves had the characteristic of being visible only when the interfacial region would try and 'flatten' just before the cycle would reverse (see movie 1). The waves usually had small amplitudes and exhibited a larger frequency than the Faraday waves. In figure 8 a photograph of such waves is shown in contrast to their 'mother' Faraday waves displayed in figure 6(*b*). The appearance of secondary or higher order waves is not a mystery. Secondary and higher harmonic waves are to be expected before cycles reverse since incorporation of smaller wavelengths and smaller amplitudes is how waves attain a means of 'flatness' during cycle reversing.

In addition to many of the earlier observations it is interesting to note that the motion was associated with standing waves with an oscillation frequency f_0, half that of the cell frequency f, i.e. $f_0 = f/2$. This important observation, seen both experimentally as well as numerically, is further evidence that the problem can be viewed as a classical Faraday problem. In this context it is noteworthy that the

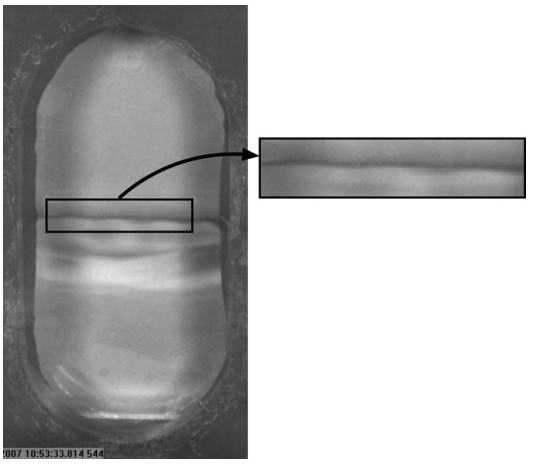

FIGURE 8. Observation of secondary wavelengths in the same oscillation but at different position. Experimental parameters: $A = 10$ cm, $f = 1.5$ Hz and $t_0 = 20$ min.

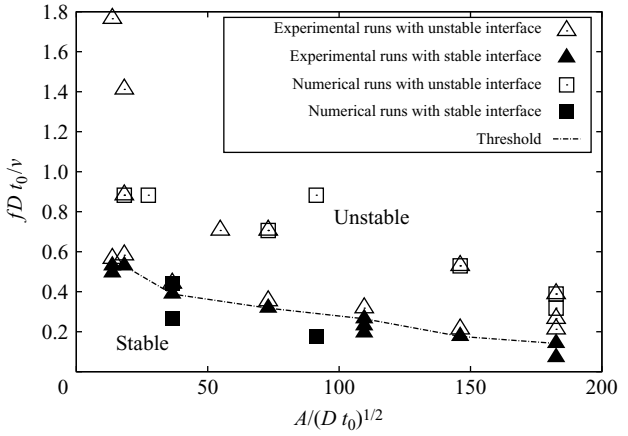

FIGURE 9. Phase diagram in the case of pure and salty water. The dashed line shows the limit of stable and unstable regions.

problem is also similar to the instability seen when a fluid is heated from above while subject to vertical oscillations. Such a problem has been shown (Shukla & Narayanan 2002) to behave like a linear pendulum whose base plate oscillates where subharmonic behaviour at resonance is an important characteristic (McLachlan 1947; Nayfeh 1981).

In all of the experiments, the onset of the Faraday instability was studied by fixing the oscillation amplitude A and gradually increasing the frequency f until the formation of a wavelength at the interface. Figure 9 shows the resulting phase diagram of the scaled frequency versus the scaled oscillation amplitude for the water/brine system. The dashed line in this figure shows the experimental threshold above which wavelengths could be observed at the interface and below which the interface remained stable. The numerical simulations and experimental runs both show that above this 'onset' curve, the various cases were unstable while below it, they were stable.

The experiments in the oil/oil systems differed in two ways from those carried out with brine and pure water. First, a higher acceleration and amplitude was required

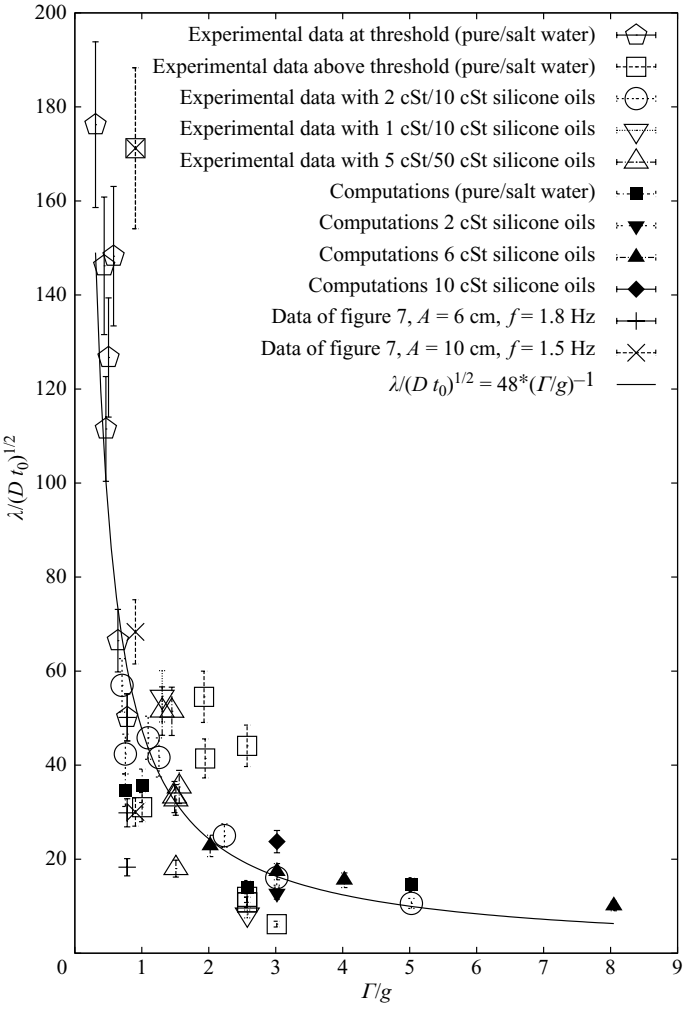

FIGURE 10. Wavelength as a function of the acceleration obtained experimentally and numerically.

in order that the instability develop. For example, for the 5 cSt/50 cSt combination, the miscible interface showed waviness for only oscillation amplitudes of $A \geqslant 5$ cm. The second difference was that the instability lasted much longer in the case of the oil/oil systems. Indeed, with viscous liquids, and in particular for the 5 cSt/50 cSt combination, the instability could be observed for tens of seconds or sometimes for more than 1 min without seeing liquid mixing whereas in the salt–saturated water experiments the instability induced mixing very rapidly due to its lower viscosity.

The main results from the experiments for the case of silicone oils and brine/pure water are summarized in figure 10 which shows the observed scaled wavelength as a function of the scaled acceleration. Several observations are made from this figure.

First, the experimental data and numerical calculations are in good agreement within the precision of the evaluation of the wavelength, especially for higher values of the acceleration.

Second, for lower values of the acceleration, the wavelength is large and for higher values of the acceleration, the wavelength is small and saturates as the acceleration increases. These observations follow from our earlier comments on the nature of the instability and the fact that large accelerations come attendant with small wavelength saturation. The deviation in the plots for the larger wavelengths is understandable on account of the interference of the side walls and the consequent departure from a clearly demarked wavenumber. To check the effect of side wall dimension, calculations were also performed for a larger width of 8 cm with no discernible change seen in the wavelengths at the onset of instability.

Third, the effect of viscosity on the developing wavelengths was of interest; therefore several experiments were carried out using silicone oil combinations of either 1 cSt/10 cSt, 2 cSt/10 cSt or 5 cSt/50 cSt. These particular combinations were chosen for their relatively small density differences (see table 1). Despite this small difference in density and the limitation in acceleration provided by our set-up, the different oil combinations developed Faraday instabilities. The key result of these experiments is that the wavelength at the onset of the instability always increased with viscosity. This result also agreed with the computations as seen in the figure and with the linearized stability results of Kumar and Tuckerman (1994) in the limit of large viscosity.

Finally, a curve fit of all of the points, both experimental and numerical yields the relation $\lambda/(Dt_0)^{1/2} = B(\Gamma/g)^b$, where $\Gamma = A(2\pi f)^2$ is the vibrational acceleration, $B \approx 48$ and $b \approx -1$. This expression is similar to the form of the dispersion relation obtained by Kumar & Tuckerman (1994). Now their study, unlike ours, dealt with the linearized Faraday instability of immiscible layers. This agreement between both studies is remarkable yet understandable since the root cause for the instability is similar in both studies even though the causes for stabilization are somewhat dissimilar. The agreement with the power law result of Kumar & Tuckerman (1994) is another important feature of our work.

5. Summary

In our experimental and numerical study of the Faraday instability of miscible interfaces several observations have been made. In the course of this a physical explanation has been advanced which suggests that the observed instability derives from an analogue of Faraday instability between miscible liquids and the stably arranged oscillating Bénard problem. Instability in miscible systems is markedly different than its immiscible counterpart on account of its transient nature as well as the lack of a clear interface. The most important results which are discussed in this study are four-fold. First, the observed threshold wavelength of the instability decreased with an increase in external threshold acceleration for various miscible fluid systems. Interestingly, this is in very good agreement with earlier published theoretical results for studies on immiscible systems in which the interfaces, in contrast with the present work, are well defined. Second, the observed frequency of the pattern was half the imposed frequency, also in agreement with earlier results on immiscible systems. Third, the wavelength of the onset patterns decreased as the waiting period to commence the external oscillations increased. Finally, the wavelength increased with the mean viscosity or in other words with the mean Schmidt number of the miscible system.

The numerical model in the current work is limited to a two-dimensional study. The experimental data were confined to runs where the proximity of the container's

vertical walls was of little concern. To investigate the effect of horizontal dimensions would require both a three-dimensional numerical model as well as a re-configuration of the experimental cell, neither of which is within the scope of this study. The current work has however been able to delineate the physics of the Faraday instability in miscible fluids and to explain its characteristics and the dependence of wavelengths on system parameters.

The authors thank P. Kurowski and P. Petitjeans for their support in this project. F. Zoueshtiagh and S. Amiroudine also gratefully acknowledge the financial and computing support from CNES. R. Narayanan thanks Arts et Métiers Paris Tech. and the Partner University Fund for supporting this collaborative research.

REFERENCES

Amiroudine, S., Bontoux, P., Larroude, P., Gilly, B. & Zappoli, B. 2001 Direct numerical simulation of instabilities in a two-dimensional near-critical fluid layer heated from below. *J. Fluid Mech.* **442**, 119–140.

Amiroudine, S., Ouazzani, J., Carles, P. & Zappoli, B. 1997 Numerical solutions of 1-D unsteady near-critical fluid flows using finite volume methods. *Eur. J. Mech. B-Fluids* **16** (5), 665–680.

Amiroudine, S. & Zappoli, B. 2003 Piston-effect-induced thermal oscillations at the Rayleigh–Benard threshold in supercritical He-3. *Phys. Rev. Lett.* **90** (10).

Ballesta, P. & Manneville, S. 2006 Shear-thickening induced by Faraday waves in dilute wormlike micelles. *Europhys. Lett.* **76** (3), 429–435.

Benjamin, T. B. & Ursell, F. 1954 The stability of the plane free surface of a liquid in vertical periodic motion. In *Proc. R. Soc. Lond. A* **225** (1163), 505–515.

Faraday, M. 1831 On the forms and states of fluids on vibrating elastic surfaces. *Phil. Trans. R. Soc. Lond.* **121**, 319–340.

Fauve, S., Kumar, K., Laroche, C., Beyssens, D. & Garrabos, Y. 1992 Parametric instability of a liquid–vapor interface close to the critical point. *Phys. Rev. Lett.* **68**, 3160.

James, A. J., Vukasinovic, B., Smith, M. K. & Glezer, A. 2003 Vibration-induced drop atomization and bursting. *J. Fluid Mech.* **476**, 1–28.

Kumar, S. & Matar, O. K. 2004 On the Faraday instability in a surfactant-covered liquid. *Phys. Fluids* **16** (1), 39–46.

Kumar, K. & Tuckerman, L. S. 1994 Parametric instability of the interface between two fluids. *J. Fluid Mech.* **329**, 49–68.

Lide, D. R. 2004 *CRC Handbook of Chemistry and Physics*, edn 85. Taylor and Francis.

McLachlan, N. W. 1947 *Theory and Application of Mathieu Functions*. Oxford University Press.

Nayfeh, A. H. 1981 *Introduction to Perturbation Techniques*. Wiley Interscience.

Patankar, S. 1980 *Numerical Heat Transfer and Fluid Flows*. McGraw Hill.

Shukla, P. K. & Narayanan, R. 2002 The effect of time-dependent gravity with multiple frequencies on the thermal convective stability of a fluid layer. *Intl J. Heat Mass Transfer* **45** (19), 4011–4020.

Tipton, C. R. & Mullin, T. 2004 An experimental study of Faraday waves formed on the interface between two immiscible liquids. *Phys. Fluids* **16** (7), 2336–2341.

Ubal, S., Giavedoni, M. D. & Saita, F. A. 2005*a* Elastic effects of an insoluble surfactant on the onset of two-dimensional Faraday waves: a numerical experiment. *J. Fluid Mech.* **524**, 305–329.

Ubal, S., Giavedoni, M. D. & Saita, F. A. 2005*b* The formation of Faraday waves on a liquid covered with an insoluble surfactant: Influence of the surface equation of state. *Latin Am. Appl. Res.* **35** (1), 59–66.

Zoueshtiagh, F., Legendre, M., Caps, H., Vandewalle, N., Petitjeans, Ph. & Kurowski, P. 2006 Air bubbles under vertical vibrations. *Eur. Phys. J.* E **20**, 317–325.